OMAE2021-61939

DYNAMIC MODEL DEVELOPMENT OF WIND TURBINE DRIVETRAINS BY USING SENSOR MEASUREMENTS

Diederik van Binsbergen[*]**, Amir R. Nejad**
Department of Marine Technology
Norwegian University of Science and Technology (NTNU)
Trondheim, Trøndelag, 7052
Norway
Email: dirk.w.van.binsbergen@ntnu.no

Jan Helsen
Department of Mechanical Engineering
Vrije Universiteit Brussel (VUB)
Brussel, 1050 Elsene
Belgium

ABSTRACT

This paper aims to analyze the feasibility of establishing a dynamic drivetrain model from condition monitoring measurements. In this study SCADA data and further sensor data is analyzed from a 1.5MW wind turbine, provided by the National Renewable Energy Laboratory. A multibody model of the drivetrain is made and simulation based sensors are placed on bearings to look at the possibility to obtain geometrical and modal properties from simulation based vibration sensors. Results show that the axial proxy sensor did not provide any usable system information due to its application purpose. SCADA data did not meet the Nyquist frequency and cannot be used to determine geometrical or modal properties. Strain gauges on the shaft can provide the shaft rotational frequency, while torque and angular displacement sensors can provide the torsional eigenfrequency of the system. Simulation based vibration sensors are able to capture gear mesh frequencies, harmonics, sideband frequencies and shaft rotational frequencies.

NOMENCLATURE

OPEX   Operational Expenditure
LCOE   Levelized Cost Of Energy
SCADA   Supervisory Control And Data Acquisition
CMS   Condition Monitoring System
RUL   Remaining Useful Life
OEM   Original Equipment Manufacturer

DOF   Degree Of Freedom
EMA   Experimental Modal Analysis
OMA   Operational Modal Analysis
p-LSCF   Polyreference Least-Square Complex Frequency-Domain
SSI-COV   Covariance-Driven Stochastic Subspace Identification
K   Stiffness
C   Damping
M   Moment
F   Force
T_{gen} Generator Torque
K_P Proportional Gain Parameter
K_I Integral Gain Parameter
ω Angular Velocity
MBS   Multibody Simulation
F   Frequency
LC   Load Case
DLC   Design Load Case
LVRT   Low Voltage Ride Through
FFT   Fast Fourier Transform
PSD   Power Spectral Density
INP-A   Main Shaft Bearing
PLC-A,B   Planet Carrier Bearings
PL-A,B   Planet Bearings
IS-A,B,C   Intermediate Shaft Bearings
HS-A,B,C   Highspeed Shaft Bearings
GS-A,B,C   Generator Shaft Bearings
GS 1,2,3   Gear Stage
MS   Main Shaft
ISS   Intermediate Speed Shaft
HSS   High Speed Shaft
GS   Generator Shaft

---

[*]Address all correspondence to this author.

1 INTRODUCTION

Wind turbines are increasing in size and are moving further offshore which results in longer downtime and an increase in cost [1]. Especially the downtime per failure of drivetrain components, such as the gearbox and bearings, seems to be significantly long. Optimizing maintenance strategies where failure could be predicted can help with predictive maintenance or life extension and will subsequently reduce the operational expenditure (OPEX) and the levelized cost of energy (LCOE).

Condition monitoring with the use of turbine supervisory control and data acquisition (SCADA) and condition monitoring systems (CMS) can be used to actively track system properties and can aid in early detection of faults in the drivetrain of the wind turbine. Data-driven CMS have been used for early fault detection but lack the possibility of prognosis due to its "black-box" approach where no physical knowledge is known regarding the failure mechanism [2]. Using a physics of failure approach, where damage accumulation is modeled using a physical model, can potentially result in more accurate results and can result in a better understanding of the underlying failure mechanics.

While turbine manufacturers know every single detail of their turbine design, operators often lack sufficient information to be able to make a physical model of the wind turbine which could be used for the physics of failure approach.

The objective of this work is to analyze the feasibility of establishing a dynamic drivetrain model from condition monitoring measurements which, in the future, can be used for a physics of failure approach condition monitoring system, subsequently and ultimately being used for prognosis and remaining useful life (RUL) estimation. The possibility of model creation for wind turbine operators will be investigated and an evaluation will be made on which sensors can be used for which drivetrain parameters. Different types of sensors are analyzed on a 1.5MW case study wind turbine drivetrain and a case study drivetrain model.

The structure of the paper is as follows: First in Subsections 1.1-1.6 a brief literature review will be done in order to describe the state-of-the-art. Section 2 will describe the methodology. Then, Section 3 shows and discusses the results and in Section 4 concluding remarks will be made and future work will be proposed.

1.1 State-Of-The-Art

The following Subsections consists of a brief review on condition monitoring based on the physics of failure approach in Subsection 1.2. Then, in Subsection 1.3 the data availability for operators will be reviewed and discussed. In Subsection 1.4 the recommended model fidelity for the drivetrain will be reviewed. Subsection 1.5 reviews the modal behaviour of the drivetrain assembly and reviews the proposed model fidelity of a wind turbine drivetrain. A review will be done on methods used to determine modal parameters and finally various load cases and its effect on

system identification will be discussed in Subsection 1.6.

1.2 Physics Based Condition Monitoring

Condition monitoring with the use of turbine SCADA and vibration measurements can be used for early fault detection of wind turbine components and is already shown to work, as shown in Weinert et al. [2]. However, prognosis is still a large challenge, especially when data-driven methods are used.

While physics based condition monitoring for wind turbines is not that widely used, various other industries already looked at the application of physics based condition monitoring [3]. For this specific case a physics based model is made for applications in the aerospace industry from a lumped parameter finite element model, which is widely used to model the helicopter transmission.

Gray and Watson [4] presented a physics of failure approach for wind turbine condition monitoring where the force under static conditions was assumed to be directly proportional to the torque transferred between the rotor and the generator with a correction applied for peak contact stresses acting on gearbox bearings. Lundberg-Palmgren theory was then further used to find the bearing fatigue life and the Palmgren-Miner rule is applied for bearing damage accumulation. The Kaplan-Meier estimator is then used to determine the the Weibull shape and scale parameters to convert the damage accumulation into a probability of failure.

In Breteler et al. [5] a physics of failure methodology was proposed, which was divided into three parts: detection, diagnostics and prognostics, where data considered for this work was either from the SCADA or CMS. For the detection part the misalignment of the shaft is measured with a laser to be used for the lifetime calculation. For the diagnostics part the ISO standards are used to determine the root bending stress on the gears. Similar to Gray and Watson, the Palmgren-Miner rule is then applied for the bearing damage accumulation calculation. For prognostics the damage accumulation is plotted against the time. In total the accumulation is measured for three wind turbines, showing a large difference in lifetime consumption between each turbine, which is explained due to the difference in wind speed per wind turbine.

Physics based condition monitoring can potentially better represent damage development and give more accurate results, although due to a lack of studies the full potential is not reached yet [2].

1.3 Data Availability for Operators

It is common that wind turbine operators cannot install their preferred monitoring systems within the manufacturer's warranty period [6]. Also, wind turbine operators generally do not have enough information available to develop a physical model of the drivetrain of a wind turbine, making modal analysis, model

creation and prognosis even more challenging. It is mentioned in Breteler et al. (2015) [5] that a large amount of parameters should be known to achieve a sufficient model accuracy, which can be difficult to acquire for the operator. Even though operators are trying to find solutions for the lack of data by sharing turbine data with each other [7], there is still a significant gap of turbine knowledge between operator and the original equipment manufacturer (OEM).

1.4 Proposed Model Fidelity

In order to model the wind turbine drivetrain, it should first be decided what fidelity level is needed in order to accurately model the drivetrain behaviour, while maintaining a relatively low computational time. Yi Guo et al. (2015) [8] did a literature review on the modeling approaches available, subdividing it into three classes:

1. Low fidelity : Analytical, lumped-parameter modeling
2. Intermediate fidelity : Multibody dynamic tools
3. High fidelity : Finite element tools

This work will be taken into account during the modeling phase of the case study drivetrain.

1.5 Gearbox Modal Characteristics

In order to tune the wind turbine drivetrain model, modal analysis can be applied on the data acquired from the sensors of the case study wind turbine.

Modal analysis is the process of determining the inherent dynamic characteristics of a system in forms of natural frequencies, damping factors and mode shapes [9].

For design it is of importance to know the turbine dynamics to minimize overlap of resonance and excitation frequencies, ultimately resulting in less fatigue damage.

For turbine operators it is important to know the turbine dynamics to design and tune the model, which subsequently could be used for various advanced condition monitoring purposes.

Different methodologies are developed to calculate modal characteristics of drivetrains and various literature is released on the modal behaviour of drivetrain components of a wind turbine.

For a three degree of freedom (DOF) lumped parameter model the planetary stage modes can be found in translational and rotational direction for the carrier, ring and sun [10], while no planet modes exist for a gearbox with three planets [11]. For a six DOF model the out of plane modes, consisting of tilt modes and axial modes, is added [12].

The shafts consist of mode shapes that result in rotations or axial translations of each shaft [13]. Furthermore, every shaft consists of multiple torsional and bending modes, each able to be excited by a specific eigenfrequency.

These modes and eigenfrequencies can be determined by experimental modal analysis (EMA) and operational modal analysis (OMA). EMA is performed in a simulated controlled environment, while OMA is performed when the system is in operation [14].

OMA has already been proven useful in various industries and is increasingly used in the wind energy sector on the blades [15,16], the tower [17,18] and the drivetrain [19,20] and the possibility of tracking modal parameters on drivetrain components has also been investigated [21,22].

One of the main OMA assumptions concerning the excitation is that it is distributed randomly both in time and space. While wind is traditionally assumed to obey this OMA assumption, Tcherniak et al. (2011) [17] concluded that due to rotor rotation, this assumption is not met and can result in inaccurate results at the rotational frequency. In order to reduce the influence of the harmonic content, Daems et al (2021) [20] applied a cepstrum-based time-domain signal editing procedure [23], reducing the influence of deterministic content, while preserving the modal content. Three different modal parameter estimation algorithms were used, being the p-LSCF (Polymax), PolyMax Plus and the SSI-COV method.

Elkafafy et al. (2017,2019) [21,22] applied a modal tracking methodology, where the damped natural frequency and damping ratio are tracked over a longer time using the operational p-LSCF (Polymax) estimator, not needing any preprocessing due to the idle state of the turbine.

Gioia et al. (2019) [19] demonstrated a methodology where multiple hours of vibration data were autonomously processed and applied a data-driven modeling tool on the data to find correlations between estimated modal parameters and the operational settings of the turbine. Results showed that correlations between the estimated modal parameters and the turbine operational setting could be found.

1.6 Influence of Load Cases on System Identification

In order to find the system properties of the drivetrain, various load cases are considered which can be found in IEC61400-1 [24]. Load cases with a sudden change in operation and control are known to result in undesirable load effects on dynamic components of the drivetrain. These transient responses contain different system information compared to steady-state responses [25]. Thus both the transient load cases and steady-state load cases should be analyzed for system identification. The case study wind turbine used in this work is a 1.5MW wind turbine. Information on this wind turbine is available in NREL/TP-5000-70639 [26], NREL/TP-5000-71529 [27], NREL/TP-5000-63679 [28] and in Guo and Keller (2020) [29]. Experimental data is provided by NREL [30] and is publicly available. Load cases used and further information will be giving in Section 2.

2 METHODOLOGY

The methodology of this work starts with describing the case study wind turbine, wind turbine drivetrain and the wind turbine drivetrain model in Subsection 2.1. Then in Subsection 2.2 the different sensors that will be analyzed are mentioned. In Subsection 2.3 the analyzed load cases are shown and finally the data tools used to analyze the data is shown in Subsection 2.4.

2.1 Case Study Wind Turbine

The case study wind turbine concerns the 1.5MW NREL turbine [26–28]. The 1.5MW drivetrain design is based on IEC 61400-4 [31] where a 3-stage gearbox is used with one planetary stage and two parallel stages with helical gearing [27]. The gearbox rating is 1660 KW with an input rated rotor speed of 18.39 RPM and gearbox ratio of 78.292.

The high speed shaft (HSS) is designed for a rated speed of 1440 RPM and torque of 10.25 kNm. 3 bearings support the high speed shaft, starting with one bearing towards the rotor side and two towards the generator side.

A schematic layout of the gearbox can be seen in Figure 1, where the main shaft is located to the left and the generater shaft is located to the right. The Cartesian coordinate system is used.
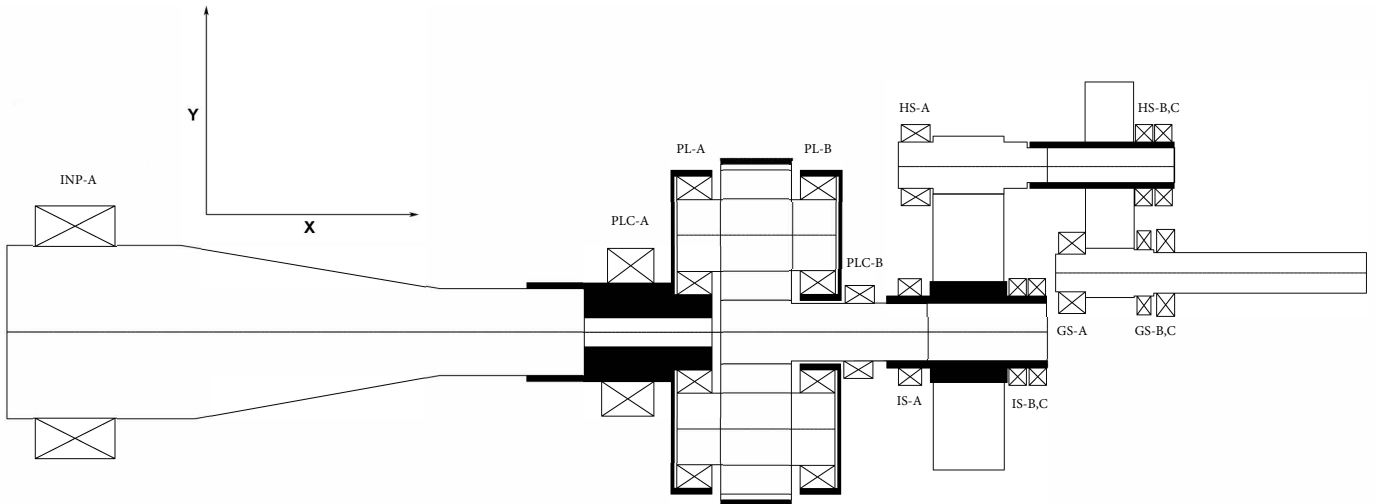
Gear Pair. The gears are modeled as rigid bodies with elastic gear teeth composed of stiffness, damping and frictions terms, where the stiffness is calculated based on DIN 3990 Method B and the damping is proportional to the stiffness.

The bearings are modeled using linear diagonal stiffness-and damping matrices shown in Equation 1. The damping value is taken as 1% of the stiffness value [34], while the stiffness values are based on [35] and [36], where k_{xx}, k_{yy} and k_{zz} represent axial, tangential and radial stiffness in N/m and corresponding damping values in Ns/m and $k_{\alpha\alpha}$, $k_{\beta\beta}$ and $k_{\gamma\gamma}$ represent the rotational direction, corresponding to a stiffness of 0 Nm/rad, of the shaft and the pitch and yaw direction of the wind turbine and corresponding damping values in Nms/rad.

$$\mathbf{K} = \begin{pmatrix} k_{xx} & 0 & 0 & 0 & 0 & 0 \\ 0 & k_{yy} & 0 & 0 & 0 & 0 \\ 0 & 0 & k_{zz} & 0 & 0 & 0 \\ 0 & 0 & 0 & k_{\alpha\alpha} & 0 & 0 \\ 0 & 0 & 0 & 0 & k_{\beta\beta} & 0 \\ 0 & 0 & 0 & 0 & 0 & k_{\gamma\gamma} \end{pmatrix}, \mathbf{C} = \begin{pmatrix} c_{xx} & 0 & 0 & 0 & 0 & 0 \\ 0 & c_{yy} & 0 & 0 & 0 & 0 \\ 0 & 0 & c_{zz} & 0 & 0 & 0 \\ 0 & 0 & 0 & c_{\alpha\alpha} & 0 & 0 \\ 0 & 0 & 0 & 0 & c_{\beta\beta} & 0 \\ 0 & 0 & 0 & 0 & 0 & c_{\gamma\gamma} \end{pmatrix}$$

(1)

FIGURE 1. Case study: Gearbox schematic layout

Further information has been provided by NREL and is used to make a multibody model of the drivetrain from the case study wind turbine. Each bearing is supplied with a simulation based sensor. These sensors are able to capture the bearing acceleration, velocity and displacement in each direction.

KISSsoft [32] is used for sizing of each gear stage. The gears are then modeled in SIMPACK [33] as force element, FE225:

The shafts, bedplate and gearbox housing are modeled as rigid components.

Input loads are provided by NREL [30]. The thrust load, F_x, is based on the power production, F_y is assumed to be 0 and F_z is based on the weight of the blades. The torque, M_x, is provided, the overturning moment, M_y, can be calculated from the blade weight and M_z is assumed to be 0.

The generator torque is modeled as a proportional-integral velocity controller applied on the generator shaft, which is shown in Equation 2:

$$T_{gen} = K_P(\omega - \omega_{ref}) + K_I \int_0^t (\omega - \omega_{ref})dt \qquad (2)$$

Where ω is the angular velocity of the generator shaft obtained from the multibody simulation (MBS) model and ω_{ref} is the angular velocity found from sensors on the wind turbine.

A top view of the SIMPACK model can be seen in Figure 2. Input loads are applied on the main shaft, on the rotor side of the INP-A bearing, while generator torque is applied on the high speed shaft, towards the generator side.
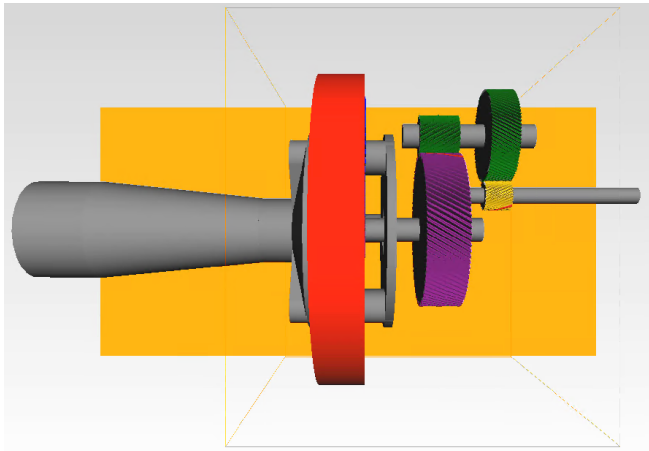

FIGURE 2. Case study: Top view of the gearbox multibody model

2.2 Drivetrain Sensors

In this work, the following sensor outputs are considered:

-SCADA system
-Axial proxy sensor
-Strain gauges
-Torque and angular displacement sensors

In addition to the sensors on the physical turbine, the SIM-PACK model is provided with simulation based sensors.

SCADA system The SCADA system provides data at a frequency of 1 Hz for all basic knowledge an operator should need to successfully control the wind turbine.

Axial Proxy Sensor The axial proxy sensor was installed on the main bearing housing to originally analyze main bearing axial movement for different load cases (LC) [30]. The axial proxy sensor provides data at a frequency of 5000 Hz.

Strain Gauges The strain gauges were applied to determine the torque and the bending moment [26] on the high speed shaft. The strain gauges give data at a frequency of 5000 Hz.

Torque and Angular Displacement Sensors The main shaft is supplied with a torque measurement sensor and the high speed shaft is supplied with an angular displacement sensor. These sensors sampling frequency is in the order of 50 Hz at rated.

Simulation Based Sensor The sensors applied on the bearings in the model measure displacements, velocities and accelerations on each bearing in X, Y and Z direction. The sampling frequency is chosen to be 1000 Hz.

2.3 Load cases

The load cases [24,30] evaluated for the physical sensors are the following:

LC_1: Normal Operation (DLC_1)
LC_2: Low Voltage Ride Through (LVRT, $DLC_{2.5}$)
LC_3: Start Up (DLC_3)
LC_4: Shut down ($DLC_{4,5}$)
LC_5: Idle (DLC_6)

Each sensor for each load case is analyzed using signal processing methods discussed in Subsection 2.4.

2.4 Data Analysis Methods

On signals with a clear oscillating frequency and large amplitude in time domain, the peak counting method will be applied.

For the remaining data the following frequency domain methods are used in combination with Welch's method in order to find system properties of the drivetrain:

-Fast Fourier Transform (FFT)
-Power Spectral Density (PSD)
-Spectrogram
-Campbell Diagram

Further more, the proxy sensor data was preprocessed due to an excursion caused by a locknut slot [27].

3 RESULTS AND DISCUSSION

The results from the sensors mentioned in Subsection 2.2 will be presented in Subsection 3.1, starting with the SCADA system and the proxy sensors. Then, the strain gauges, torque and angular displacement sensor. Finally, the simulation sensors applied on each bearing will be mentioned.

In the results section for frequency domain methods, only Campbell diagrams will be shown. Campbell diagrams are easy to interpret and are applicable for load cases that heavily vary in rotational speed such as start-up and shut down.

3.1 Sensor Results

SCADA system The SCADA system is unable to capture any eigenfrequencies and harmonics due to its limited sampling frequency.

Axial Proxy Sensors The main bearing axial proxy sensors are analyzed for each load case, LC_1-LC_5, for each data analyzing method. Results show no indication that any system property could be found from these sensors for this specific placement. Most sensors show constant, noisy, excitation frequencies, even in Campbell diagrams. Different placement could give better results.

Strain Gauges Figure 3 shows the Campbell diagram of a strain gauge placed on the generator shaft, which were originally used to calculate the bending moment and the torque [26]. On the X-axis the main shaft rotational frequency is plotted, while on the Y-axis the generator shaft rotational frequency divided by the gearbox ratio is plotted. A clear peak can be seen on the line $y = x$ with a slope of 1, where the signal gets more visible with an increase in rotational speed. Using a tachometer is the conventional way to determine the rotational speed of a shaft. However, when the system does not provide any data on the rotational speed of the shaft and the gearbox ratio is unknown, it shows that also strain gauges can be used to determine the rotational speed of the shaft. Other than the rotational speed of the shaft, no other system properties can be found using shaft strain gauges in this layout. The placement of this sensor is important, since whether a sensor is placed on a shaft node or not will significantly affect results. Also the direction of the strain gauge will give different results.

Torque and Angular Displacement Sensors The torsional eigenfrequency can be determined in different ways.
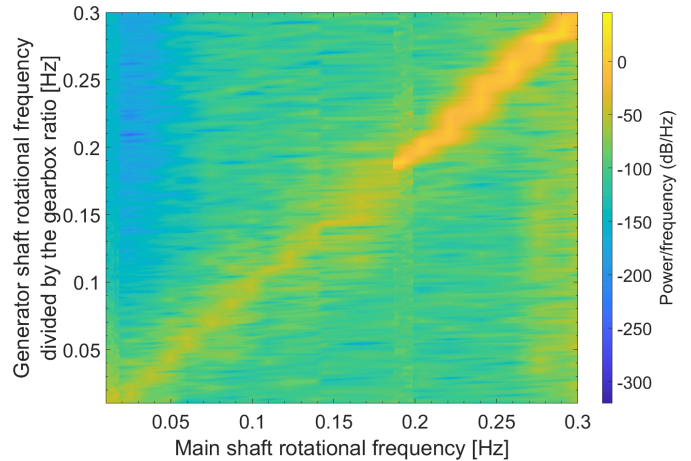
FIGURE 3. Campbell diagram of the generator shaft strain gauge B_Y

Khazaeli and Nejad (2020) [37] showed that the torsional eigenfrequency of the system can be determined by the use of two angular velocity sensors, one placed on the main shaft and one on the generator shaft.

In this work the torsional eigenfrequency of the system is determined by analyzing either the main shaft torque sensor or the high speed shaft angular displacement sensor. From the high speed shaft angular displacement sensor the main shaft rotational speed is determined. The torsional eigenfrequency is determined using a transient load case, such as a LVRT ($DLC_{2.5}$), a turbine start-up (DLC_3) or a turbine shut down ($DLC_{4,5}$). Figure 4 shows the main shaft speed and main shaft torque with the occurence of a LVRT, which is induced by a 50% voltage drop [27]. This results in a torque drop and will subsequently result in an increased shaft rotational speed, since the generator torsional resistance decreases while the rotor blades still provide torque. Both the torque and the shaft speed will then fluctuate on the first torsional eigenfrequency of the system until it slowly dampens out. By counting the peaks of either the torque or the shaft speed, the eigenfrequency can then be found.

The top plot of Figure 4 shows the main shaft speed in *rpm* measured by an angular displacement sensor and the SCADA system. The occurence of the LVRT is unnoticeable for the SCADA system due to its limited sampling frequency of 1 *hz*, not meeting the Nyquist frequency. The middle plot shows the main shaft torque, while the bottom plot shows the FFT based on the main shaft torque during the LVRT.

The resulting system torsional eigenfrequency that is found by counting the peaks corresponds with the FFT and is $F_n = 2.07 Hz$.
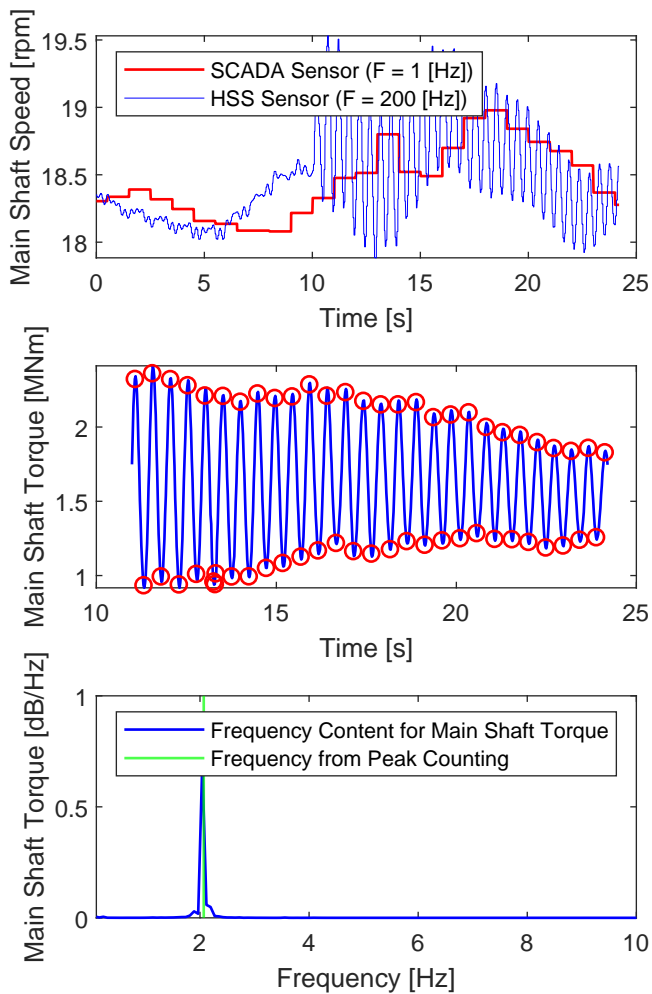
FIGURE 4. Torsional Eigenfrequency Identification

Simulation Based Sensors The acceleration measured by the sensors placed on bearings, which layout is shown in in Figure 1, are analyzed in axial (X) and radial (Y,Z) direction. Mainly Campbell diagrams are used to analyze the sensor data for each load case. Start-up and shutdown load cases are analyzed in Campbell diagrams due to their change in rotational speed over time. A shutdown load case ($DLC_{4,5}$) has been used to produce the upcoming Figures. Different bearings on the same shaft did not give significantly different results due to the rigid shafting assumption. No bearing properties were found due to them being modeled as linear diagonal stiffness/damping matrices.

The theoretical gear meshing frequencies, harmonics and

sidebands are calculated and then compared with the simulation results. When a clear indication of a signal is present in the Campbell diagram, the corresponding line is plotted on top of the signal, to give a more clear view of the obtained results.

Main Shaft The main shaft consists of the INP-A and PLC-A bearings. In Figure 5 the Campbell diagram of the INP-A bearing in radial (Y) direction is shown. The Campbell diagram shows the gear meshing frequency of the first stage with multiple harmonics.
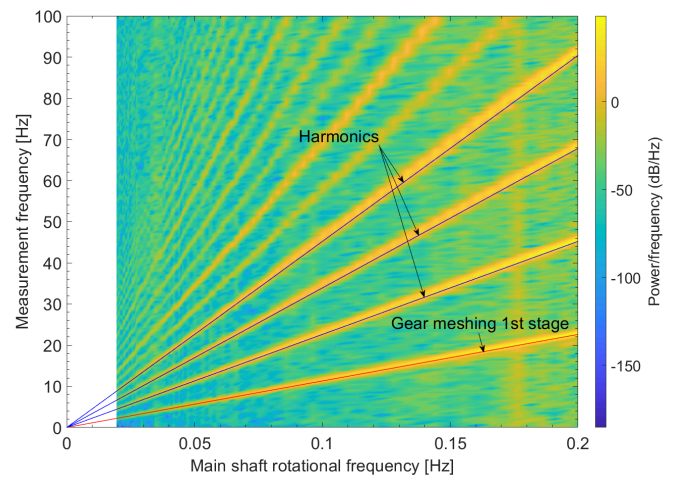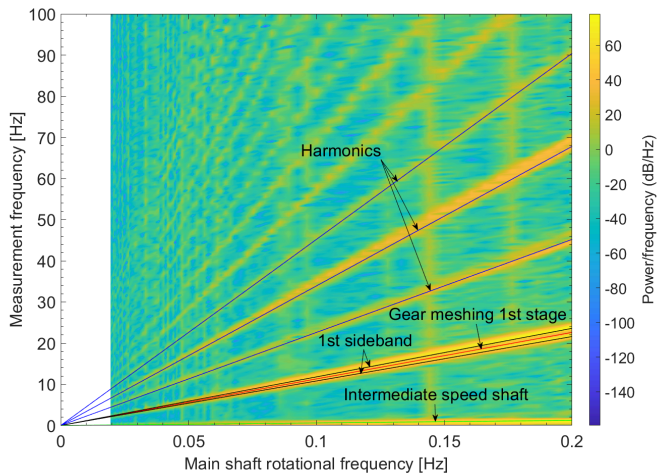

FIGURE 5. Campbell diagram of the INP-A bearing in radial (Y) direction

Planet Shaft The gearbox assembly consists of three planet shafts, one for each planet bearing. The sensors on the bearings of the planet shaft did not result in any identifiable system frequencies.

Intermediate Speed Shaft The intermediate speed shaft consists of the PLC-B and IS-A,B,C bearings. In Figure 6 the Campbell diagram of the IS-A bearing in radial (Z) direction is shown. The Campbell diagram did not specifically show the gear meshing frequency of the first stage, but did show the first lower and higher sideband frequency of the gear meshing with multiple harmonics. It also shows the shaft rotational speed.
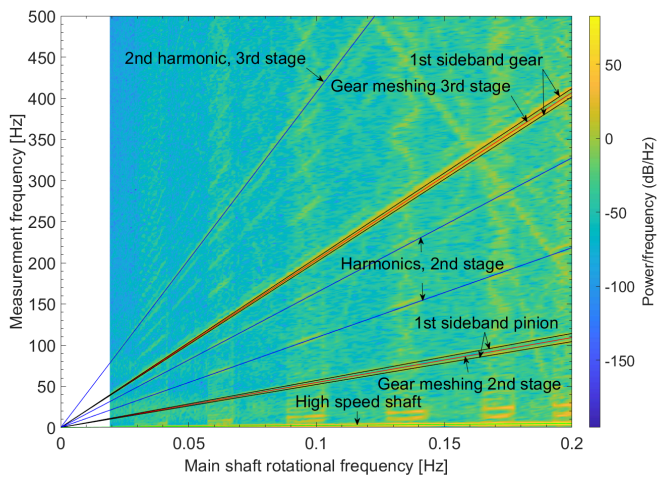
High Speed Shaft The high speed shaft consists of the HS-A,B,C bearings. In Figure 7 the Campbell diagram of the
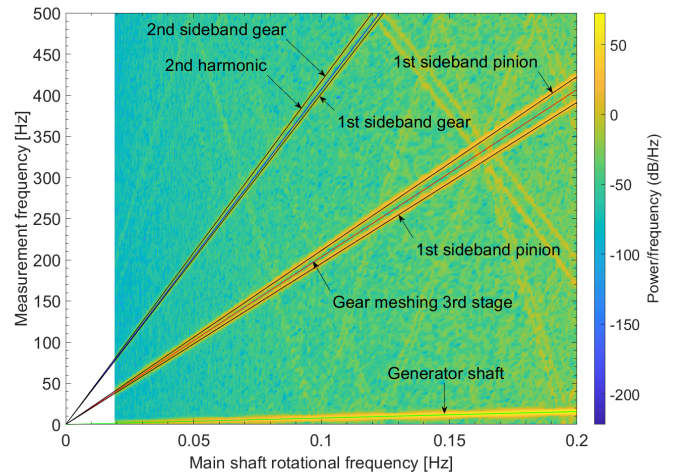
FIGURE 6. Campbell diagram of the IS-A bearing in radial (Z) direction

HS-A bearing in radial (Z) direction is shown. Both the sidebands of the gear meshing of the second and third stage can be seen in the Figure, where for the second stage the pinion sidebands were found, while for the third stage the gear sidebands were found. Also harmonics could be found for each gear meshing frequency and the shaft rotational speed can be seen on the lower side of the Figure.

FIGURE 7. Campbell diagram of the HS-A bearing in radial (Z) direction

Generator Shaft The generator shaft consists of the GS-A,B,C bearings. In Figure 8 the Campbell diagram of the GS-A bearing in radial (Z) direction is shown. Again, the gear mesh frequency of the specific stage could not be seen in the Figure, while sideband frequencies could be seen. Where in Figure 7 the gear sidebands were found, in Figure 8 the pinion sidebands were found. Also, only the harmonics of the sideband frequencies were found, but these did not correspond with the exact sideband frequencies found around the meshing frequency. Similar to the ISS and HSS, the generator shaft frequency could be found.

FIGURE 8. Campbell diagram of the GS-A bearing in radial (Z) direction

from the Campbell diagrams, most system parameters could be extracted. Gear meshing frequencies are very useful to determine the gear ratio and in combination with the sidebands, the exact transmission ratio for helical stages, including number of teeth, can be found. For a planetary stage determining the system properties can be a larger challenge due to the amount of variables. Where a helical stage consists of two gears, a planetary stage consists at least out of one sun gear, which could be floating or not, three or more planetary gears and a ring gear. Further more, in reality, when bearing frequencies and noise will be part of the signal, identification can become more challenging.

For establishing a dynamic drivetrain model, the acceleration sensors give by far most information. However, it should be noted that these sensors are simulation based, while in reality the sensor might be subject to various other signals and noise.

Having the gear meshing and sideband frequencies, the gear ratio and its number of teeth can be calculated. Using the torsional eigenfrequency, the shaft layout can be estimated and the rotational speed of the shaft can be used as check to validate

8

the found gear ratio per stage. Most gear properties can then be estimated using the rated power and rated torque, found from SCADA measurements. In future work this will be further elaborated.

There will be a trade off between cost and amount of available data when for system identification. On a limited budget not each bearing can be provided with vibration sensors.

4 CONCLUSION AND FUTURE WORK

This study looks at the possibility to identify system properties from sensors installed by NREL on a 1.5MW wind turbine. SCADA data is analyzed but does not meet the Nyquist frequency. Axial proxy sensors on the main bearing are analyzed and do not give any system properties. Strain gauges on the high speed shaft can provide the shaft rotational frequency and torque and displacement sensors can provide the torsional eigenfrequency of the system. A multibody gearbox model is created and each bearing is supplied with a simulation based acceleration sensor. Results show that from these sensors the shaft rotational frequency, gear meshing frequencies, harmonics and sideband frequencies of each gear pair can be found.

Future work will be to increase the model fidelity and validate the results found. Furthermore, a flow chart for operators will be introduced aiding operators into the design of a dynamic drivetrain model, which ultimately can be used for prognosis purposes and remaining useful life estimation.

REFERENCES

[1] Faulstich, S., Hahn, B., and Tavner, P. J., 2011. "Wind turbine downtime and its importance for offshore deployment". *Wind Energy, 14*(3), pp. 327–337.

[2] Tautz-Weinert, J., and Watson, S. J., 2017. "Using scada data for wind turbine condition monitoring – a review". *Iet Renewable Power Generation, 11*, pp. 382–394.

[3] Stringer, D., Sheth, P., and Allaire, P., 2012. "Physics-based modeling strategies for diagnostic and prognostic application in aerospace systems". *Journal of Intelligent Manufacturing, 23*, 04, pp. 155–162.

[4] Gray, C. S., and Watson, S. J., 2010. "Physics of failure approach to wind turbine condition based maintenance". *Wind Energy, 13*(5), pp. 395–405.

[5] Breteler, D., Kaidis, C., Tinga, T., and Loendersloot, R., 2015. "Physics based methodology for wind turbine failure detection, diagnostics prognostics".

[6] Kuseyri, S., 2015. "Condition monitoring of wind turbines: Challenges and opportunities".

[7] Bungane, B. New data-sharing project to enhance the efficiency of wind turbine operators. https://www.smart-energy.com/renewable-energy/new-data-sharing-project-to-enhance-the-efficiency-of-wind-turbine-operators/. [Online; accessed 22-Feb.-2021].

[8] Guo, Y., Keller, J., Cava, W. L., Austin, J., Nejad, A. R., Halse, C., Bastard, L., and Helsen, J., 2015. "Recommendations on model fidelity for wind turbine gearbox simulations".

[9] He, J., and Fu, Z.-F., 2001. "1 - overview of modal analysis". In *Modal Analysis*, J. He and Z.-F. Fu, eds. Butterworth-Heinemann, Oxford, pp. 1–11.

[10] Parker, R. G., and Wu, X., 2010. "Vibration modes of planetary gears with unequally spaced planets and an elastic ring gear". *Journal of Sound and Vibration, 329*(11), pp. 2265–2275.

[11] Lin, J., and Parker, R., 1999. "Analytical characterization of the unique properties of planetary gear free vibration". *Journal of Vibration and Acoustics, 121*, 07.

[12] Eritenel, T., and Parker, R. G., 2009. "Modal properties of three-dimensional helical planetary gears". *Journal of Sound and Vibration, 325*(1), pp. 397–420.

[13] Helsen, J., 2012. The dynamics of high power density gear units with focus on the wind turbine application,,(het dynamisch gedrag van hoge vermogensdichtheidstandwielkasten toegepast op windturbines).

[14] Bin Zahid, F., Chao, O., and Khoo, S., 2020. "A review of operational modal analysis techniques for in-service modal identification". *Journal of the Brazilian Society of Mechanical Sciences and Engineering, 42*, 08.

[15] Marulo, F., Petrone, G., D'Alessandro, V., and Di Lorenzo, E., 2014. "Operational modal analysis on a wind turbine blade". pp. 783–797.

[16] Brüel & Kjær, Branner, K., and Buhl, T. Operational modal analysis on wind turbine blades. https://www.bksv.com/-/media/literature/Case-Study/bn1630.ashx.

[17] Tcherniak, D., Chauhan, S., and Hansen, M., 2011. *Applicability Limits of Operational Modal Analysis to Operational Wind Turbines*, Vol. 1. 07, pp. 317–327.

[18] Chauhan, S., Tcherniak, D., Basurko, J., Salgado, O., Urresti, I., Carcangiu, C., and Rossetti, M., 2011. *Operational Modal Analysis of Operating Wind Turbines: Application to Measured Data*, Vol. 5. 03, pp. 65–81.

[19] Gioia, N., Daems, P.-J., Peeters, C., Guillaume, P., Helsen,

J., Medico, R., Deschrijver, D., and Dhaene, T., 2019. "Gaining insight in wind turbine drivetrain dynamics by means of automatic operational modal analysis combined with machine learning algorithms".

[20] Daems, P.-J., Peeters, C., Guillaume, P., and Helsen, J., 2021. *Operational Modal Analysis of Wind Turbine Drivetrain with Focus on Damping Extraction*. 01, pp. 399–405.

[21] Elkafafy, M., Devriendt, C., Guillaume, P., and Helsen, J., 2017. "Automatic tracking of the modal parameters of an offshore wind turbine drivetrain system". *Energies, 10*, 04, p. 574.

[22] Elkafafy, M., Gioia, N., Guillaume, P., and Helsen, J., 2019. *Long-Term Automatic Tracking of the Modal Parameters of an Offshore Wind Turbine Drivetrain System in Standstill Condition*. 01, pp. 91–99.

[23] Randall, R., Antoni, J., and Smith, W., 2019. "A survey of the application of the cepstrum to structural modal analysis". *Mechanical Systems and Signal Processing, 118*, pp. 716–741.

[24] International Electrotechnical Commision (IEC), 2019. *Wind turbines - Part 1: Design requirements for fixed offshore wind turbines*.

[25] Dalen, C., and Ruscio, D., 2016. "On closed loop transient response system identification". *Modeling, Identification and Control: A Norwegian Research Bulletin, 37*, 01, pp. 213–223.

[26] Keller, J., and Lambert, S., 2019. Gearbox Instrumentation for the Investigation of Bearing Axial Cracking. Technical Report NREL/TP-5000-70639, National Renewable Energy Laboratory. [Online; accessed 10-Dec.-2020].

[27] Keller, J., Guo, Y., and Sethuraman, L., 2019. Uptower Investigation of Main and High-Speed-Shaft Bearing Reliability. Technical Report NREL/TP-5000-71529, National Renewable Energy Laboratory. [Online; accessed 10-Dec.-2020].

[28] Santos, R., and van Dam, J., 2015. Mechanical Loads Test Report for the U.S. Department of Energy 1.5-Megawatt Wind Turbine. Technical Report NREL/TP-5000-63679, National Renewable Energy Laboratory. [Online; accessed 10-Dec.-2020].

[29] Guo, Y., and Keller, J., 2020. "Validation of combined analytical methods to predict slip in cylindrical roller bearings". *Tribology International, 148*, p. 106347.

[30] Keller, J., 2020. DRC-uptower measurements. https://nrel.app.box.com/s/fx1wu3pkvgbeu5ikv7ghn61pjg1oao20. [Online; accessed 08-Dec.-2020].

[31] International Electrotechnical Commision (IEC), 2012. *Wind turbines - Part 4: Design requirements for wind turbine gearboxes*.

[32] Kisssoft ag. https://www.kisssoft.com/en. [Online; accessed 10-Dec.-2020].

[33] Dassault systemes - multibody system simulation software. https://www.3ds.com/products-services/simulia/products/simpack/. [Online; accessed 10-Dec.-2020].

[34] Nakhaeinejad, M., and Bryant, M., 2011. "Dynamic modeling of rolling element bearings with surface contact defects using bond graphs". *Journal of Tribology-transactions of The Asme, 133*, p. 011102.

[35] Nejad, A. R., Guo, Y., Gao, Z., and Moan, T., 2016. "Development of a 5 mw reference gearbox for offshore wind turbines". *Wind Energy, 19*(6), pp. 1089–1106.

[36] Wang, S., Nejad, A. R., and Moan, T., 2020. "On design, modelling, and analysis of a 10-mw medium-speed drivetrain for offshore wind turbines". *Wind Energy, 23*(4), pp. 1099–1117.

[37] Khazaeli, F., and R. Nejad, A., 2020. "Natural frequency estimation by using torsional response, and applications for wind turbine drivetrain fault diagnosis". *Journal of Physics: Conference Series, 1618*, 09, p. 022019.